Journal of Thermal Analysis and Calorimetry (2019) 138:2515–2528
https://doi.org/10.1007/s10973-019-08593-y

Thermal analysis and microstructure of oxide dispersion strengthened ferritic steels produced by ball milling with different amounts of process control agent

V. Mihalache[1] · G. Aldica[1] · I. Pasuk[1] · I. Mercioniu[1]

Received: 4 November 2018 / Accepted: 19 July 2019 / Published online: 30 July 2019

Abstract
Fe–14Cr–3 W–0.4Ti–0.25Y_2O_3 ferritic steels were produced by ball milling of initial mixture of elemental powders with various amounts of process control agent (PCA), ethanol (0.25 mass%, 2.5 mass%, 4 mass% and 20 mass%) under an Ar atmosphere and spark plasma sintering (SPS) consolidation at 1070 °C. The influence of the quantity of PCA on the properties (microstructure, density and Vickers hardness) of the as-milled powders and of the consolidated steels was investigated. X-ray diffraction shows a bcc–α-phase with fine crystallite size, 6.7–11 nm, for all powders. The particle size and the lattice constant of α-ferrite of the as-milled powders decrease as the amount of PCA increases. The powder milled with the highest amount of PCA, 20 mass%, contains carbides (M_3C) and oxides ($(Fe,Cr)_2O_3$). The thermal analysis shows that as the amount of PCA increases, (1) the Curie temperature, T_c, increases, (2) the temperature of $\alpha \rightarrow \gamma$ transition, $T_{\alpha\rightarrow\gamma}$, decreases, (3) the mass loss with CO/CO_2 degassing increases, and (4) the milling with PCA hinders the nitrogen incorporation from milling media and air. The density and Vickers hardness of the SPS-consolidated and post-SPS annealed steels show an increasing trend with the increase in the amount of PCA. Carbides and oxides were detected in the post-SPS annealed steels derived from the powders milled with 2.5 mass% PCA and 4 mass% PCA ($M_{23}C_6$ and $(Fe,Cr)_2O_3$), and 20 mass% PCA (M_3C and $(Fe,Cr)_2O_3$). The obtained results were discussed in terms of: (1) dissolution into the alloy matrix of carbon and oxygen released after the disintegration of PCA, (2) carbides and oxides precipitation during milling and/or upon heating and (3) promotion of thermally activated processes (such as carbothermal reaction) upon heating which can develop as well at the contact points/particle surfaces during SPS consolidation and can influence the process of densification.

Keywords ODS Fe14Cr ferritic steel · Ball milling · Process control agent · Thermal analysis · Microstructure · Density · Vickers hardness

Introduction

High oxidation resistance and microstructural and mechanical stability to heat of ferritic stainless steels provide an attractive cost–performance ratio for production of components and structural materials to be exposed to elevated and high temperatures for applications covering a broad spectrum of domains (e.g., nuclear power plants [1], automotive industry [2], food-processing industry [3], etc.). In particular, a promising application of oxide dispersion strengthened ferritic steels, ODSFSs, is as structural materials in fission and fusion power reactors (e.g., first wall and breeding blanket) [1]. In order to enhance the high-temperature mechanical properties of ODSFS, a nanostructuring induced by mechanical alloying is required. Long-time (over 40 h) and/or high-energy milling is necessary for efficient dry ball milling. In these conditions, the impurification of powders from air during milling is nearly inherent when the mill is placed under an atmospheric environment and the contamination can occur even if the powders were loaded under an inert (e.g., argon) atmosphere [4, 5]. The contamination with nitrogen and

✉ V. Mihalache
valentina.mihalache@infim.ro

[1] National Institute of Materials Physics, PO Box MG 7, 77125 Magurele, Romania

oxygen is supposed to be caused by the leakage of air through the seals into the container during milling [6 references therein]. In our previous works [4, 5], we have demonstrated that the contamination of Fe–14Cr–3 W–0.4Ti–0.25Y_2O_3 ferritic steel powders with nitrogen and oxygen uptaken from air can occur during dry milling—up to 0.5 mass% nitrogen can be incorporated after 100–170 h of milling time in the optimum milling conditions, under an Ar atmosphere and without interruption of the milling process. An efficient method to avoid contamination from air is to place the mill inside a glove box maintained under a high-purity inert gas atmosphere [6 and references therein]. In this case, however, during long-term dry milling, the powders might be contaminated with carbon from the container walls/balls [6 and references therein]; the impurification is difficult to register by conventional measurement techniques, such as XRD and SEM/EDS, because the contamination level is under the detection limit of these apparatus. The intentional introduction of different amounts of carbon during milling can be a viable method for investigation and understanding the influence of carbon contamination on the properties of the final steel. If the carbon will be introduced through the process control agent (PCA), it will allow as well investigating the influence of milling with different amounts of PCA on the powder quality as well as on the final steel quality. The PCA used in mechanical alloying MA by ball milling influences considerably the powder morphology, particle size and consequently their densification behavior [6–8]. In particular, PCA adsorbed on the newly formed fractured surfaces in the milling process, lowers their surface tension and prevents particle agglomeration and their coarsening. An advantage of milling with PCA in respect of dry milling is that finer particles with more homogeneous size distribution can be obtained and a shorter milling time is required to reach the desired grain (crystallite) size. The spark plasma (SPS) is a time-saving method of sintering; shorter time exposure to high temperatures—high pressure conditions—prevents the grain coarsening and preserves their intrinsic properties. It also makes possible to produce highly dense compacts at lower (nominal) temperatures.

Within this work, the milling with different amounts of ethanol was applied on Fe–14Cr–3W–0.4Ti–0.25Y_2O_3 powders in the aim to understand the influence of the quantity of PCA (carbon and oxygen) on the microstructure, thermal properties, density and Vickers hardness of the as-milled powders and SPS-consolidated steels. The amounts of carbon and oxygen (PCA) introduced into the initial powders were known, and the secondary phases and the thermally activated processes were easier to detect (by XRD, TG/DTA and mass spectrometry, MS, measurements) in the products derived from the powders milled with high amounts of PCA. This facilitated understanding and interpretation of the behavior of the products derived from the powders milled with a very low amounts of (or even without) PCA—the product consolidated from the powder milled with the lowest amount of PCA (0.25 mass%) contains carbon, nitrogen and oxygen in quantities close to those uptaken from the container walls and balls and/or from air during long-time dry milling. In addition, the results of highly sensitive TG/DTA (combined with MS) measurements obtained in this work can help to choose the optimum temperature for degassing, consolidation, annealing and/or for reducing oxides/carbides if they are not desired. The results of this work could be of interest for any Fe–Cr-based alloys.

Experimental

Elemental powders of iron (99.9%, metal bases), chromium (99.2%, metal bases), tungsten (99.9%, metal bases), titanium (99.5%, metal bases) and Y_2O_3 (produced by sol–gel technique) were weighted in the 85.35:14:0.3:0.4:0.25 mass% ratios, respectively, and mechanically alloyed in a planetary ball mill (Retsch) using hardened steel (with chromium and carbon in the composition) balls and containers. The milling process parameters were chosen as follows: the ratio of the mass of the balls to the powder (BPR)—10:1, milling speed—450–550 rpm (with direction reversal and 15 min pause time after every 10 min running time), total effective milling time—49 to 60 h, milling atmosphere—Ar, process control agent (PCA)—ethanol (CH_3CH_2OH): 0.25 mass%, 2.5 mass%, 4 mass% and 20 mass%, Y_2O_3 powders were produced by sol–gel technique using precursors based on acetates and propionic acid [9]. The vials were sealed (under an Ar atmosphere) using an O-ring of a circular cross section. The powders will be referred to as P0.25, P2.5, P4 and P20.

For the consolidation of MA powders, a commercial SPS machine (FCT Systeme GmbH–HP D 5, Germany) was used. The powders (about 28 g) were wrapped into a C-paper (FCT Systeme GmbH, thickness 0.04 cm) loaded into a 3.08-cm-diameter graphite die and were processed by spark plasma sintering (SPS) at 1070 °C for 5 min. The heating rate was 150 °C min^{-1}, and the cooling time was approximately 5 min. The uniaxial pressure applied on the punches was 48 MPa. The initial vacuum in the furnace was 30–40 Pa. A pulsed current pattern of 12-on/2-off pulses was applied, with a 3 ms period. The operating voltage and the peak current were below 5 V and 1600 A, respectively. The consolidated steels were thoroughly polished to remove the surface graphite contamination. The consolidated steels will be referred to as C0.25, C2.5, C4 and C20. The annealing of as-milled powders and of SPS-consolidated steels was performed in a quartz tube furnace

at 525–1150 °C for 30 min in an atmosphere of 95% Ar and 5% H_2. The annealed steels will be referred to as A0.25, A2.5, A4 and A20.

Carbon, oxygen and nitrogen analyses were performed on the consolidated steels by the inert gas fusion method using a Leco TC- 400 equipment. (Carbon, oxygen and nitrogen contents in the as-milled powders do not differ significantly from that in the consolidated steels determined by LECO since the mass loss (degassing) registered during SPS consolidation was insignificant for all the samples). The density was determined using the Archimedes method, by immersing the samples in water. XRD measurements were taken on a Bruker D8 Advance diffractometer in Bragg–Brentano geometry. Qualitative phase analysis and the estimation of the average crystallite size and lattice constants were performed by full-powder-pattern fitting using the Bruker-TOPAS software and a corundum reference sample (NIST SRM 1976) to estimate the instrumental line profiles. For SEM/EDS characterization, a TESCAN LYRA 3 XMU microscope (accelerating voltage between 5 and 30 kV) was used. SEM investigation was performed on the as-milled powders and on fractures of the SPS-consolidated steels. Thermal analysis was performed using a modular simultaneous thermal analyzer SETARAM Setsys Evolution 18 apparatus coupled with a quadrupole mass spectrometer, MS, (Pfeiffer Vacuum). About 150 mg of the as-milled powders was loaded into an open cylindrical alumina crucible. The experiments were conducted in Ar of 5 N (99.999%) purity at a flow rate of 16 mL min^{-1}. The temperature scan was performed between 25 and 1350 °C at a heating and cooling rate of 10 °C min^{-1} with a temperature precision of better than 0.01 °C. Vickers microhardness was measured on mirror polished surfaces using a PMT 3 testing instrument with a diamond pyramid indenter. A load of 100 g was applied for 5 s on polished surfaces. The microhardness for each steel was averaged over a minimum of twelve indents.

Results and discussion

Microstructure and thermal properties of powders milled with different amounts of PCA

The X-ray diffraction patterns for Fe14Cr as-milled powders are shown in Fig. 1a. Only the phase of *bcc*–α-structure appears in P0.25, P2.5 and P4 powders. For the P20 powder milled with the highest amount of PCA, the reflections of M_3C and $(Fe,Cr)_2O_3$ phases were also registered. The *bcc*–α-peaks shift toward lower 2θ as the amount of PCA increases. The diffraction lines broaden toward low 2Θ (viewed as a shoulder on *bcc*–α-peaks). A

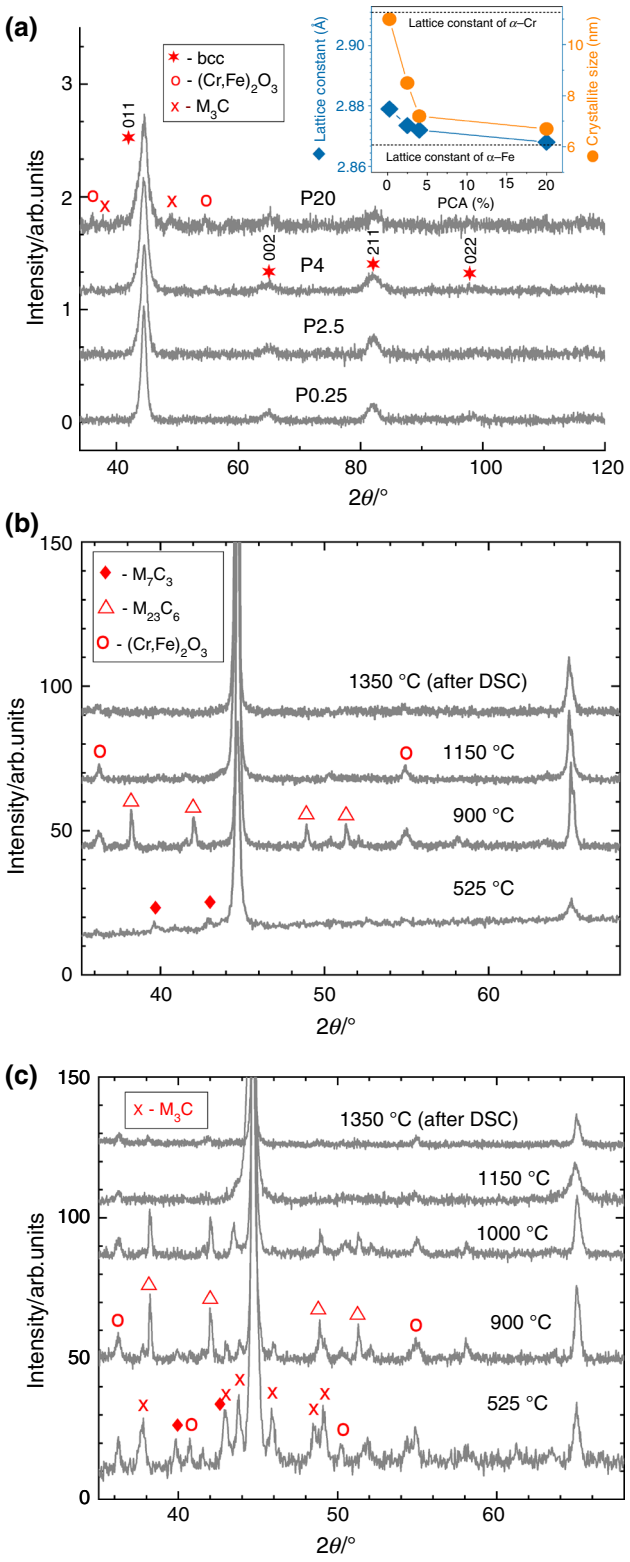

Fig. 1 XRD patterns of the **a** mechanically alloyed P0.25, P2.5, P4 and P20 powders, **b** P4 and **c** P20 powders furnace annealed at different temperatures

Table 1 Lattice constant and average crystallite size of α-bcc of as-milled, SPS-consolidated and post-SPS-annealed steels. Relative density and Vickers hardness of the SPS-consolidated and annealed ferritic steels

Powder	Milling time/h	PCA/mass%	Crystallite size/nm	Lattice constant/Å	SPS consolidated					Annealed				
					Steel	Temperature/°C	Density/g cm^{-3}	Vickers hardness/HV	Crystallite size/nm	Steel	Density/g cm^{-3})	Vickers hardness/HV	Crystallite size/nm	Lattice constant/Å
P0.25	60	0.25	11	2.879	C0.25	1070	7.31	913.3	22.3	A0.25	7.29	531.9	41	2.877
P2.5	49	2.5	8.5	2.873	C2.5	1070	7.52	1015.7	13.5	A2.5	7.47	515.8	29	2.876
P4	49	4.0	7.2	2.872	C4	1070	7.60	1160.7	12.8	A4	7.54	565.7	32	2.872
P20	60	20	6.7	2.868	C20	1070	7.32	1136.3	12.3	A20	7.23	828.2	26	2.868

remarkable refinement of crystallite size was reached (Table 1). The crystallite size of P0.25 is 11 nm (Table 1) and decreases as the amount of PCA increases (Fig. 1a inset). For P20, the crystallite size was reduced to 6.7 nm (Table 1). As seen from the inset of Fig. 1a, the lattice constant of the *bcc*–α-phase is higher compared to α-Fe and lower compared to α-Cr, and this confirms the occurrence of the alloying process of Fe–Cr. The observed decrease in the lattice constant of *bcc*-α with the increase in the amount of PCA (Fig. 1a inset) was caused by carbides and oxides precipitation during milling and thus by the Cr depletion of the ferritic matrix. The proof of this claim is the presence of carbides and oxides in P20 obtained by milling with the highest amount of PCA (Fig. 1a).

Based on these results as well as on the results reported on dry milling [4, 10] and on the short-time milling with high amount of PCA [11], the process of allowing and contamination can be described as follows. The early stage of milling implies the process of plastic deformation and fracturing of powder particles, the rate of fracturing being higher than the rate of welding. The change in microstructure during milling (Fig. 1a, Table 1) is associated with the creation and accumulation of defects (dislocations, GBs, stacking faults, interfaces, etc.) and with the mixing between the alloying elements [12, 13]. The use of PCA improves substantially the fracture rate and grain refinement because the adsorbed ethanol molecules passivate the freshly formed fractured surfaces and prevent particle agglomeration and coarsening; at long-time milling, as soon as all the PCA was adsorbed, the further reduction in particle size can lead to a high number of unpassivated surfaces which can react with PCA molecules [10 and references therein]. The decomposition products (e.g., carbon and oxygen), released after the disintegration of PCA molecules, can accumulate at the defects (GBs, dislocations, etc.), can enter interstitially resulting in interstitial solid solutions or can precipitate/nucleate as fine metallic oxides and carbides. In fact, as soon as all the PCA molecules were adsorbed, the further milling can be regarded as a dry milling. The dry milling implies the increases in the rate of welding which can increase the particle size. On the other hand, the long-time milling with a high amount of C and O can result in the solid solution- and/or precipitation-hardening of particles. The excessive increase in hardening improves particle embrittlement, and thus, fracture rate can increase again decreasing the particles size. The reduction in the particle size with the increase in the amount of PCA is evident from the SEM micrograph as shown in Fig. 2—the particle size of P20 powder (0.5–40 μm) (Fig. 2a) obtained by milling with the highest amount of PCA decreases substantially when compared with P0.25 (5–50 μm) (Fig. 2b) obtained by milling with the lowest amount of PCA. Even though no

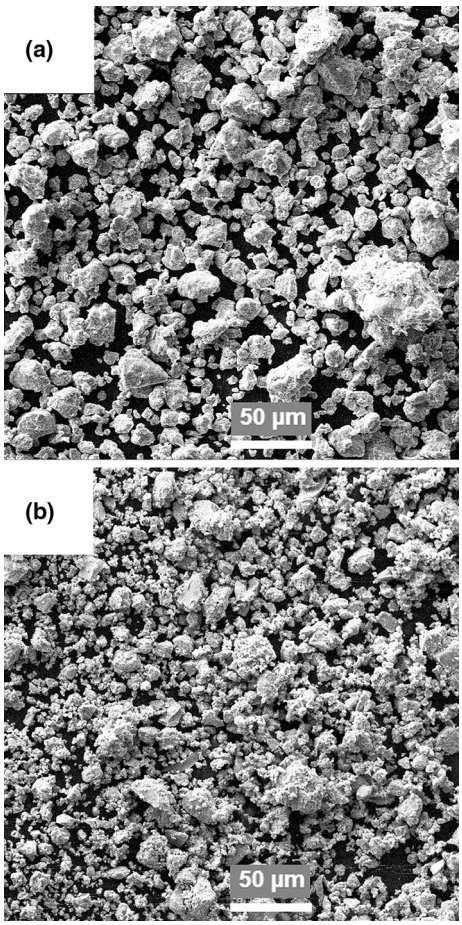

Fig. 2 SEM images of the mechanically alloyed **a** P0.25 and **b** P20 powders

secondary phases in the powders milled with up to 4 mass% PCA were detected by XRD (Fig. 1a), the contamination was evidenced by thermal analysis on as-milled powders (Fig. 3b–d), by LECO on consolidated steels (Table 2), and by XRD on annealed powders (Fig. 1b and c) and steels (Fig. 5). The increase in TG mass loss with increasing amount of PCA caused by CO/CO_2 degassing is very evident from Fig. 3b–d (will be discussed in more details hereinafter). Figure 3d and Table 2 were completed with the data on P0 powder obtained by dry milling [10] for 80 h, P30 powder milled with 30 mass% PCA for short time, 23 h [11] and C0 steel SPS consolidated from P0 powder. (From our observations (unpublished results), the longer pause time during milling (in this work, 15 min pause time after every 10 min running time was applied) implies a higher rate of contamination with nitrogen and oxygen from air. At the same duration of milling but more shorter pause time in the milling process described in ref [10] (1 min pause time was applied after every 10 min running time), the contamination rate with nitrogen was slower. That is, we choose the powder milled for 80 h, not for 50–60 h, as a representative for dry milling for comparison purposes.)

Thus, the broadening of the diffraction lines toward low 2Θ (Fig. 1a) can be associated with the metastable α-phase supersaturated with carbon most probably coexisting with the above-mentioned fine precipitates of secondary phases. The results of LECO analysis (Table 2) for the C0.25 steel consolidated from the powder P0.25 show the presence of 0.324 mass% nitrogen which is very close to 0.4 mass% nitrogen in C0 steel (consolidated from P0 powder obtained by dry milling). Thus, the quality of P0.25 is a result of simultaneous effect of carbon uptake from PCA and nitrogen uptaken from milling media and/or air during milling. The milling with nitrogen contaminants was described in details in our previous works [4, 5, 10]; the milling with nitrogen can result in interstitial nitrogen, fine precipitates of nitrides and fcc–γ-phase.

The DTA curves for all the samples (Fig. 3a) show an exothermic peak 1 at 490–630 °C, an endothermic peak 2 at 733–776 °C, an endothermic peak 3 at 776–950 °C and a broad endothermic feature 4 registered between 950 and 1300 °C accompanied by a mass loss in TG in the same temperature range. The mass loss occurs in two stages (steps). This is evident from the shape of the TG curve and especially from the two maxima in the dm/dT curves of all the samples (Fig. 3b). As the quantity of PCA increases, the (TG) mass loss region broadens and the amount of mass loss increases (Table 2). The increase in the amount of mass loss with the increase in the amount of PCA is illustrated in Fig. 3d.

The temperature positions of all the features (peaks) in DTA curves are dependent on the amount of PCA used in the milling process. The peak 2 corresponds to magnetic transition (Curie temperature, T_c), and the endothermic peak 3 corresponds to $\alpha \rightarrow \gamma$ transition, $T_{\alpha\rightarrow\gamma}$.

At the early stage of heating, up to ~ 850 °C, the powders undergo recovery, recrystallization and grain growth processes [10, 14–16]. The (lattice) relaxation when heating in this region is generated by the decrease in the number of defects accumulated during milling (e.g., dislocation, grain boundary density, etc.). The carbon, oxygen and nitrogen incorporated during milling can precipitate as the carbides, oxides and nitrides (or the phases precipitated during milling can stabilize and coarsen) simultaneously with the matrix lattice relaxation. In our previous studies [4, 5, 10], it was shown that during dry milling (without PCA), the contamination with nitrogen and oxygen from air is very probable and that an exothermic feature registered at about 650 °C is associated with this contamination.

The confirmation of the nitrides precipitation will be developed further in this work. Such confirmation is also given in our previous reports [4, 5, 10] (e.g., illustrated by Fig. 7 in [10], Fig. 9 in [4] in correlation with Fig. 9 in

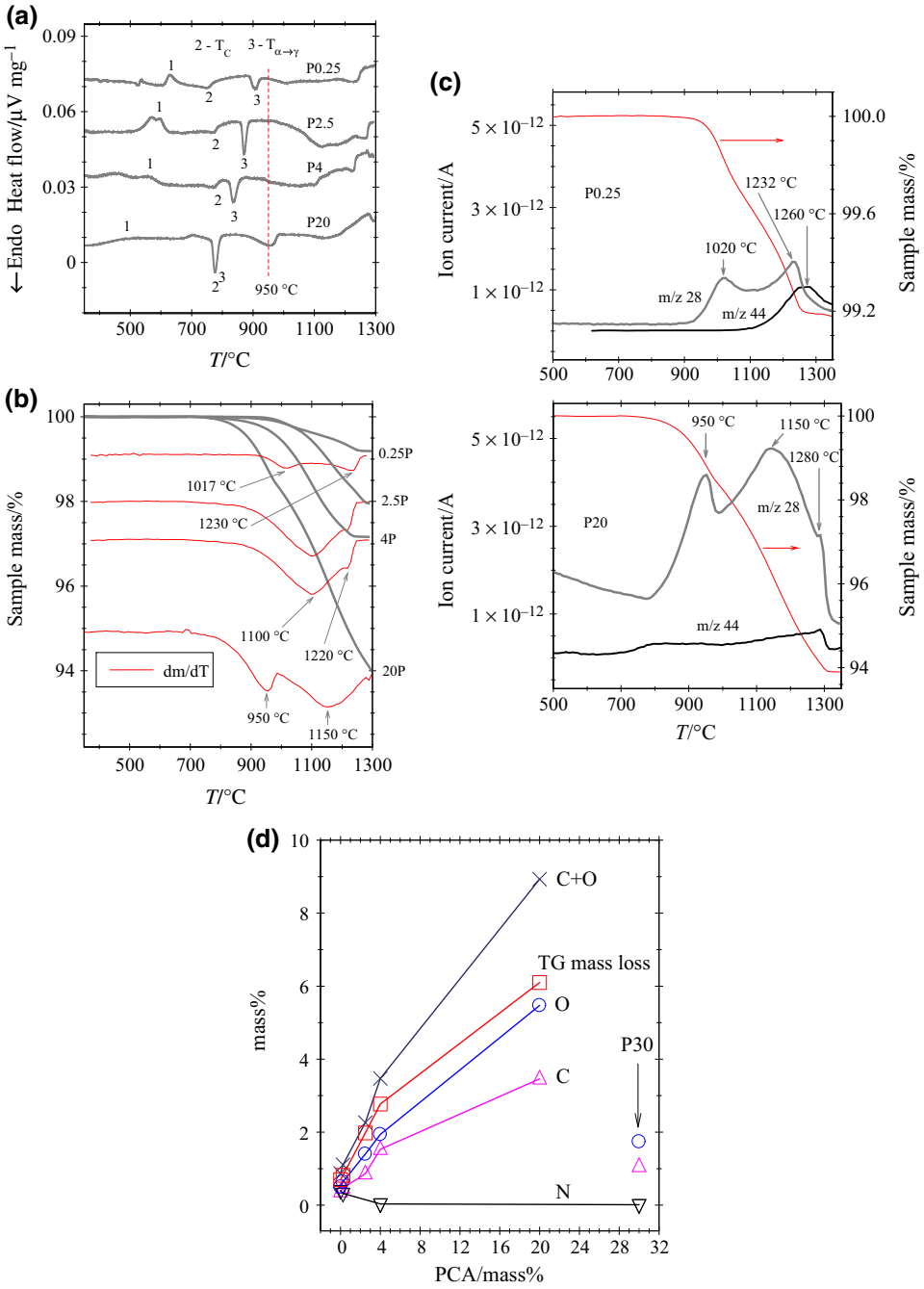

Fig. 3 Thermal analysis: **a** DTA curves for P0.25, P2.5, P4 and P20, **b** TG curves and the rate of mass loss d*m*/d*T* for P0.25, P2.5, P4 and P20, **c** the mass spectra for P0.25 and P20 and **d** the amount of C, N, O and TG mass loss (after heating to 1350 °C) as a function of PCA

[5]). In [10], XRD of heated products dry milled for long time without interruption of milling process (under an Ar atmosphere) shows Cr_2N precipitated at ~650 °C whereas an exothermic peak in the DTA heating curve was detected at the same temperature; above 900 °C, the XRD reflections for Cr_2N decrease and disappear at about 1000 °C—this decomposition of Cr_2N was accompanied by TG mass loss with a maximum rate d*m*/d*T* at the same temperature, ~1000C. In products dry milled for long time with interruption of milling process (under an Ar atmosphere), CrN has precipitated at the milling stage [4]; upon heating, the quantity of CrN diminished and vanished above 1100 °C; the decrease in intensity of CrN reflections in XRD was in good agreement with the mass loss in TG with a maximum rate at 1040 °C, whereas the presence of a maximum in mass spectroscopy for $m/Z = 28$ at the same temperature has confirmed nitrogen degassing [5]). Moreover, our preliminary study on the milling in the nitrogen atmosphere confirms the nitrides precipitation at around 600 °C (unpublished results). Thus, the peak 1 at 630 °C in

Table 2 Carbon, nitrogen and oxygen contents and the amount of TG mass loss. The amount of C, N and O for C0, C0.25, C4 and P30 was measured by LECO. C and O content in A2.5 and A20 was estimated from the reflections of carbides and oxides in XRD patterns of the annealed at 1050 °C and polished steels

Product	PCA/mass%	TG mass loss during DTA heating of as-milled powders/mass%	Contamination		
			Oxygen/mass%	Nitrogen/mass%	Carbon/mass%
C0	0	0.7	0.499 ± 0.192	0.400 ± 0.162	0.372 ± 0.048
C0.25	0.25	0.82	0.638 ± 0.020	0.324 ± 0.011	0.469 ± 0.095
A2.5	2.5	1.98	1.41 ± 0.17		0.86 ± 0.08
C4	4.0	2.77	1.94 ± 0.02	0.0323 ± 0.0009	1.53 ± 0.078
A20	20	6.1	5.47 ± 0.11		3.46 ± 0.14
P30 (23 h milling) [11]	30		1.74 ± 0.10	0.0113 ± 0.0001	1.06 ± 0.01

DTA curve for P0.25 powder obtained by milling with the lowest amount of PCA, 0.25 mass%, could be attributed to the precipitation/nucleation of nitrides (e.g., Cr_2N and/or CrN) generated by contamination with nitrogen from milling media and/or air. According [4, 5], the mass loss in TG above the $\alpha \rightarrow \gamma$ transition and the associated endothermic feature at 1000–1260 °C in DTA curve could be ascribed to the decomposition of nitrides with degassing of N_2. However, the total mass loss in TG, 0.82 mass%, for P0.25 (Table 2, Fig. 3) is much higher than the total content of nitrogen absorbed, 0.324 mass%. On the other hand, P0.25 contains 0.469 mass% carbon and 0.638 mass% oxygen suggesting that a carbothermal reduction might have contributed to the mass loss at 1000–1260 °C in TG and to the associated endothermic feature in energy. The same is valid for the P0 powder obtained by dry milling, 0 mass% PCA, since its O, C and N contents (almost the same as in C0, Table 2) are close to that of P0.25. The exothermic peak 1 reduces in the intensity, broadens and shifts to lower temperatures as the quantity of PCA increases. The decrease in the intensity of the peak 1 may indicate that the nitrogen content decreases as the amount of PCA increases, namely the milling with PCA hinders the nitrogen uptake from the air. This is in good agreement with the results of LECO analysis (Table 2): The amount of nitrogen decreases from 0.324 ± 0.011 mass% to 0.0323 ± 0.0009 mass% as the amount of PCA increases from 0.25 to 4 mass%. (The possible reasons for the decrease in contamination with nitrogen from air will be suggested later in this paper.) The broadening and the decrease in the temperature of the exothermic peak 1 as the quantity of PCA increases might be the effect of carbides, e.g., the enhanced precipitation and/or coarsening of M_3C (detected by XRD in P20 powder as shown in Fig. 1a).

The increase in the quantity of carbides (carbon) and oxides (oxygen) generated by the reaction of PCA with the powder particles during milling influences the Curie temperature, T_c, and the temperature of $\alpha \rightarrow \gamma$ transition, $T_{\alpha\rightarrow\gamma}$, (Fig. 4). To evidence the influence of nitrogen and carbon incorporated during milling (besides the effect of alloying with Cr) on these parameters, they are compared with the T_c and $T_{\alpha\rightarrow\gamma}$ of as-received Fe. T_c increases with the increase in the amount of PCA which can be explained as the reduction in Cr in Fe-rich matrix because of the nucleation/crystallization of Cr-rich secondary phases [10] such as oxides, carbides and nitrides. T_c of P2.5, P4 and P20 is very close to T_c of the as-received Fe, because it was enhanced by the precipitation of carbides and oxides. T_c of P0.25 was influenced (enhanced) by the presence of both nitrogen (Cr-rich nitrides precipitation) and carbon. The lower T_c (749 °C) for P0.25 as compared to Fe (769 °C) could be explained as the effect of alloying with Cr (Cr dissolved within the Fe matrix) prevailing over the effect of nitrides (e.g., [10] and references therein) and carbides precipitation. $T_{\alpha\rightarrow\gamma}$ behavior is a result of (besides the

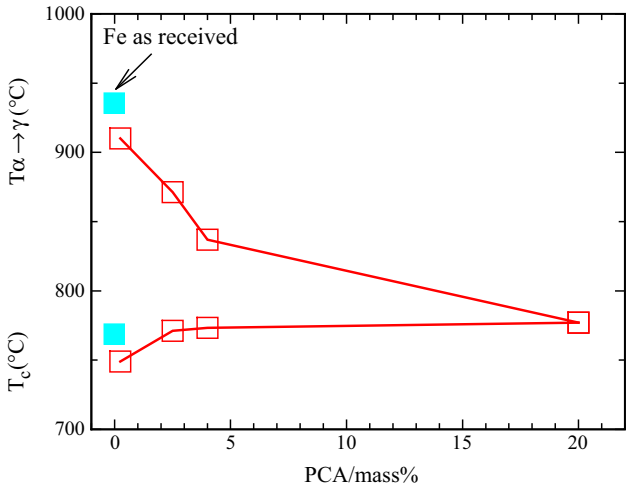

Fig. 4 Curie temperature, T_c, and the temperature of ferrite to austenite phase transition, $T_{\alpha\rightarrow\gamma}$, as a function of PCA

alloying with Cr) the different amounts of carbon and nitrogen incorporated into the ferrite matrix. $T_{\alpha\rightarrow\gamma}$ decreases with the increase in the amount of PCA (Fig. 4) enlarging the stability interval of austenite because: (i) the increased amount of incorporated carbon (Table 2); (ii) the decrease in the concentration of Cr in the ferrite matrix due to the Cr-rich carbides, nitrides and oxides precipitation [10]—according EDX with SEM investigations, the final (average) Cr-content in all the studied steels remained close to the nominal one, 14 mass% Cr, indicating that only the local concentration of Cr was changed or there is a non-homogeneous distribution of Cr within steel matrix.

As discussed herein, the carbides and oxides were registered in XRD of the as-milled P20 powder (Fig. 1a). To evaluate the processes that caused the mass loss in TG, P4 and P20 powders were annealed at different temperatures (525 °C, 900 °C, 1000 °C and 1150 °C). The powders were annealed for 30 min under an Ar–5%H2 atmosphere and furnace cooled down to RT. The evolution of secondary phases (carbides and oxides) in P4 and P20 powders with increasing annealing temperature is illustrated in Fig. 1b and 1c, respectively; the patterns after DTA (1350 °C) are also shown. XRD patterns clearly reveal the appearance of carbides and oxides in the annealed P4 powder (Fig. 1b) as compared to as-milled powder (Fig. 1a). A trace of M_7C_3 was detected at 525 °C, at 900 °C, the sharp reflections of $M_{23}C_6$ and $(Cr,Fe)_2O_3$ can be seen, and at 1150 °C, $M_{23}C_6$ vanished, whereas at 1350 °C (after DTA), the reflections of $(Cr,Fe)_2O_3$ reduced significantly. The XRD pattern of P20 annealed at 525 °C shows M_3C (but with sharper reflections as compared to the same carbide in the as-milled powder in Fig. 1a) and traces of M_7C_3; at 900–1000 °C, the sharp reflections of the same phases ($M_{23}C_6$ and $(Cr,Fe)_2O_3$) as in P4 were registered, whereas at 1150–1350 °C, these reflections reduced drastically.

The TG curves of P4 and P20 products (Fig. 3b and c) when correlated with the type of impurity phases registered by XRD in the as-milled powders (Fig. 1a) and during furnace annealing (Figs. 1b and c) suggest that the mass loss might be caused by CO/CO_2 degassing, accompanying the carbides (e.g., M_3C, $M_{23}C_6$) decomposition and/or their transformation to other more thermodynamically stable carbides, during reactions such as the carbothermal reduction in oxides.

A strong evidence of CO/CO_2 (and N_2) degassing upon heating above 950 °C is supported by mass spectrometry, MS, analysis in the temperature range up to 1350 °C. The MS for the least contaminated P0.25 product is very similar to that of the powder obtained by dry milling for long time as described in [5]. The MS curve of P0.25 product (Fig. 3c) shows a signal caused by mass 28 (associated with N_2 and CO degassing) at 1020 °C in the region of the first step in TG mass loss and a second one at higher temperature, 1232 °C, in the region of the second mass loss step. For P20, a pronounced signal with two maxima, caused by mass 28 associated with the CO degassing, was registered. The first signal occurs at 950 °C, and the second one (broader) is centered at 1150 °C—the regions were the first and second steps, respectively, in the TG mass losses occur (see also Fig. 3b). A signal caused by mass 44 (CO_2) was registered for both P0.25 and P20 samples—in the region of the second step in TG at 1260 °C for P0.25 and in the broad temperature range 750–1290 °C for P20. The intensity of *m*/*Z* 44 (CO_2) is lower than *m*/*Z* 28 (CO) for both P0.25 and P20. The intensity of *m*/*Z* 28 (CO) signal for P20 is higher by a factor of 4 than for P0.25 which is consistent with the higher amount of PCA used in the milling process of P20 powder.

The carbon, oxygen and nitrogen contents and the TG mass loss evolution with the increase in amount of PCA are illustrated in Fig. 3d. The data for C0, C0.25, C4 and P30 were taken from the results of LECO analysis presented in Table 2. The O and C contents in P2.5 and P20 were *estimated* from the XRD reflections of carbides and oxides of post-SPS annealed and polished steels, A2.5 and A20. (For this purpose, for A2.5, a very long acquisition time was applied). The results of the XRD measurements on the polished surfaces of steels post-SPS annealed for 30 min in an Ar5% H_2 atmosphere are shown in Fig. 5a. They reveal the presence of M_3C and $(Fe,Cr)_2O_3$ in A20 steel. The quantity of $(Cr, Fe)_2O_3$ decreased substantially, and weak reflections corresponding to $M_{23}Cr_6$ were registered in the XRD patterns of A2.5 and A4 steels. No carbides and oxides were detected in A0.25 by this method of measurement.

As already suggested, CO and CO_2 are most probably the products of carbides decomposition during carbothermal reactions of reduction in Fe–Cr oxides [17, 18]. For the stable Cr-based oxides, the carbothermal reaction is the main reduction mechanism. For Cr-alloyed steels, the carbothermal reduction (for efficient removal of the surface oxides) was conducted with C (admixed in the form of graphite) as the reducing agent and can be described as [17, 19]:

$$\frac{2}{n}M_mO_n + 2C = \frac{2m}{n}M + 2CO \quad (1)$$

and/or with CO gaseous reducing agents eventually added to the sintering atmosphere:

$$\frac{2}{n}M_mO_n + 2CO = \frac{2m}{n}M + 2CO_2 \quad (2)$$

According to data reported in the literature on the reduction in Fe–Cr oxides with admixed C [17, 20–22], taking as well into consideration the DTA, TG and MS

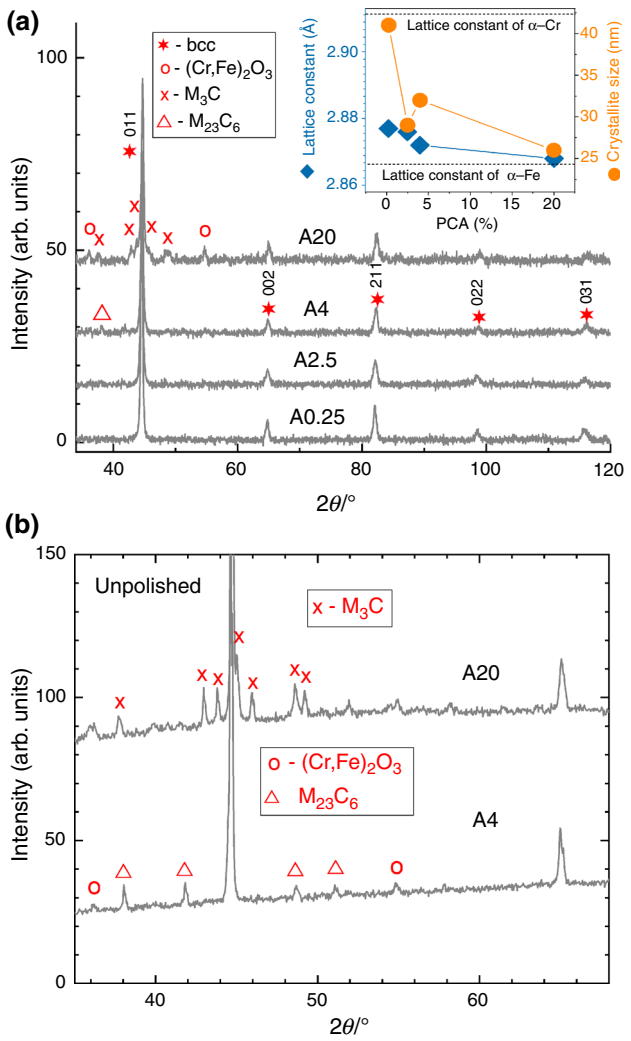

Fig. 5 XRD patterns of the post-SPS-annealed steels: **a** the polished A0.25, A2.5, A4 and A20 annealed at 1050 °C and **b** the unpolished A4 and A20 annealed at 900–1000 °C

curves (Fig. 3) correlated with the results of the XRD analysis of the annealed powders (Fig. 1b and c), it can be supposed a process of reduction in $(Fe,Cr)_2O_3$ involving the carbides and carbon as the reductant agent. At the early stage of heating of P20 powder, M_3C (segregated at the milling stage) stabilizes as a result of lattice relaxation (disordered by C and O insertion during milling). This is confirmed by sharper reflections of M_3C in XRD for P20 annealed at 525 °C (Fig. 1c) as compared to as-milled powder (Fig. 1a). A trace of M_7C_3 is also registered in the P20 powder heated at 525 °C which can nucleate at the M_3C–ferrite interface. The precipitation and/or stabilization of M_3C and M_7C_3 carbides might be the reason for occurrence of exothermic feature at about 500 °C in the DTA curve. By heating above $T_{\alpha\rightarrow\gamma}$ (Fig. 3a), M_3C becomes unstable because of the higher solubility limit of carbon in austenite; M_3C can decompose and transform to lower carbon carbide, $M_{23}C_6$ (Fig. 1c). Carbon as a product of M_3C dissolution and transformation ($M_3C \rightarrow M_{23}C_6 +$ C) can serve as a reductant agent in reduction in $(Fe,Cr)_2O_3$ and production of CO gaseous products described by:

$$(Fe,Cr)_2O_3 + C \rightarrow M + CO \quad (3)$$

Thus, M_3C and $(Fe, Cr)_2O_3$ registered in XRD for P20 were most probably involved in the reactions with CO degassing with a maximum rate at 950 °C (Fig. 3b and c). By heating at higher temperatures, above 1000 °C, $M_{23}C_6$ dissolves (Fig. 1c) and the C as a product of this dissolution can serve as a reductant agent in reaction 3. The reduction of Cr-rich oxide with carbon as the reductant agent in P20 might have contributed to the CO degassing ($m/Z = 28$) with a maximum rate at 1150 °C [17] (Fig. 3b and c). Similarly, by heating the powders milled with lower amounts of PCA at 525 °C (P4 in Fig. 1b), the ferrite matrix relax releasing the strains accumulated during milling and carbides (M_7C_3 in P4) segregate and or coarsen—these might have contributed to the exothermic feature registered at about 500-600 °C in the DTA curve (Fig. 3a); by further heating above $T_{\alpha\rightarrow\gamma}$, the lower carbon carbides ($M_{23}C_6$ in P4 at 900 °C, Fig. 1b) segregate and coarsen. These processes occurred without mass loss in TG for powders milled with a low amount of PCA. However, the decomposition of $M_{23}C_6$ when heating to higher temperatures (e.g., at 1150 °C °C for P4 in Fig. 1b) evolves the carbothermal reaction 3 resulting in the mass loss (registered in TG with a maximum rate at 1100–1230 °C (Fig. 3b)) and a degassing of CO (with a maximum at 1260 °C for P0.25, Fig. 3c). The $m/Z = 44$ (CO_2) signal registered in MS (Fig. 3c) for both P4 and P20 products suggests that CO produced in reactions 3 can further react with $(Fe,Cr)_2O_3$ [21] as follows:

$$(Fe,Cr)_2O_3 + CO \rightarrow M + CO_2 \quad (4)$$

The temperatures of carbothermal reactions 3 and 4 can overlap with the temperatures of other phenomena reported in the literature: with reactions with the liquid-phase formation [18, 24] and/or with the carbothermal reduction in the oxides from internal pores during sample shrinkage upon heating [20, 23] and/or with the reductions that are activated by the formation of a liquid phase [17]. (All these processes can contribute to the occurrence of high-temperature features registered at 1210–1300 °C in DTA, TG and MS (Fig. 3.) (This aspect is discussed in more details in our previous study [11].) Moreover, as already discussed, for the powders obtained by milling with a low amount of PCA (e.g., P0.25) as well as for the powder obtained by dry milling (e.g., P0, 0 mass% PCA), the carbothermic reduction can overlap the reactions of nitrides decomposition [4]:

$$CrN \rightarrow Cr_2N + N_2(g) \quad (5)$$

and

$$Cr_2N \rightarrow Cr + N_2(g) \quad (6)$$

or with the more complex reactions implying carbonitrides. The fact that CO_2 degassing ($m/Z = 44$) accompanies the high-temperature component (1232–1260 °C) and not the low temperature component (1020 °C) of $m/Z = 28$ can serve as an additional confirmation that the $m/Z = 28$ maximum registered at 1020 °C in DTA curve for P0.25 is due to N_2 degassing (Figs. 3a and c).

By correlating the results of LECO (Table 2), XRD (Table 1) and thermal analysis (Fig. 3a–c) summarized as well in Fig. 3d, it can be inferred that for P0.25 powder (as well as for powders obtained by dry milling) containing nitrogen and low amounts of carbon, the first mass loss step at 1020 °C is due to approximately 0.3% N_2 loss ($m/Z = 28$ in MS) caused by nitrides (precipitated at ~600 °C) decomposition according Eqs. 5 and 6. The rest of about 0.5 mass% mass loss (Figs. 3b–d) is associated with the carbothermal reactions 3 and 4 with CO ($m/Z = 28$) and CO_2 ($m/Z = 44$) degassing at 1232–1260 °C. Analogously, for P20, the first step of mass loss in TG (and the corresponding endothermic DTA peak) with a maximum rate at 950 °C is attributed to approximately 2 mass% CO and CO_2 degassing which is a result of M_3C decomposition and carbothermal reactions 3 and 4; the mass loss in TG with a maximum rate at 1150 °C (Fig. 3b and c) is due to about 4 mass% CO and CO_2 degassing as a consequence of $M_{23}C_6$ decomposition.

The results summarized in Fig. 3d indicate that about 1.1–8.9 mass% of C and O (C+O) were incorporated into the steel powder by milling with 0.25–20 mass% PCA. The contamination level of P4 (or C4) and P20 (or A20) determined by LECO (3.47 mass%) and by XRD (8.39 mass%), respectively, is in good agreement with the mass difference of powder before and after the milling (3.4 ± 0.2 for P4 and 10.2 ± 0.2 for P20). Therefore, by milling with 4 mass% PCA, about 3.4 mass% entered the steel powder and about 2.77 mass% was lost by degassing during DTA heating; by milling with 20 mass% PCA, about 10 mass% entered the steel powder and about 6.1 mass% was lost by degassing during DTA heating. During 50–60 h of high-energy milling with up to 4 mass% PCA, almost all of the PCA reacted with the powder.

According to the ethanol formula, CH_3CH_2OH, the contamination with carbon should be higher than with oxygen. However, Fig. 3d demonstrates a higher level of contamination with oxygen which is in agreement with the residual XRD reflections of the oxides registered in the powders heated to 1150–1350 °C (Fig. 1b and c). Not only PCA was the source of contamination with oxygen but also oxygen uptakes from milling media and air during milling, and especially during the holding of the sample (powder) because of the high specific area (surface-to-volume ratio) of the as-milled powders as well as the high affinity of Cr alloying element to oxygen. A relatively high level of carbon, 0.372 mass% and 0.469 mass%, registered in the C0 product (obtained from a powder P0 milled without PCA) and the powder milled with 0.25 mass% PCA, respectively, is most probably a result of the contamination from milling media and/or from air during sample holding.

The properties of steels SPS consolidated from the powders milled with different amounts of PCA

The SPS consolidation largely preserved the fine crystallite size, 12–22 nm (Table 1), of α-ferrite of the as-milled powders. (This can be also inferred from the SEM micrographs presented in Fig. 6.) The crystallite size has not increased significantly (26–41 nm) after post-consolidation annealing (Table 1). The C20 steel consolidated from P20 powder quenched to room temperature (the total quenching time of SPS-consolidated steels was about 5 min) contains M_3C and $(Fe,Cr)_2O_3$; the traces of the retained austenite were detected in the rest of the SPS-consolidated steels. The density, Vickers hardness and morphology of the consolidated and annealed steels are the results of the competition between many factors as will be described hereinafter. The increase in the quantity of carbon and oxygen with the increase in the amount of PCA during milling influenced the density, Vickers hardness [25] and morphology of the consolidated steels. As shown in Table 1, the density and Vickers hardness increase with the increase in the amount of PCA up to 4 mass%; then, they slightly decrease for 20 mass% PCA. The SEM micrographs of the fractured surfaces of SPS-consolidated C0.25 and C20 steels look very different. SEM micrograph of C0.25 (Figs. 6a and b) reveals large voids/spaces (highlighted by white arrows in Fig. 6b) denoting increased resistance to compaction of the initial powder particles. The fractured surfaces of the steels derived from the powders milled with higher amounts of PCA exhibit more compact microstructures (compare C0.25 and C20 in Fig. 6a–d) due to the finer particles of the initial powders (compare P0.25 and P20 powders in Fig. 2a and b). The pore sizes decrease, whereas their concentration increases as the amount of PCA increases (compare C0.25 and C20 in Fig. 6a–d) due to the same reason.

The interstitial solid solution and/or fine $(Fe,Cr)_2O_3$ and carbides precipitated during milling increase the particle hardness and thus hinder the efficient densification. In the case of P0.25 and P2.5, the particle hardness was also influenced by the milling with nitrogen incorporated during

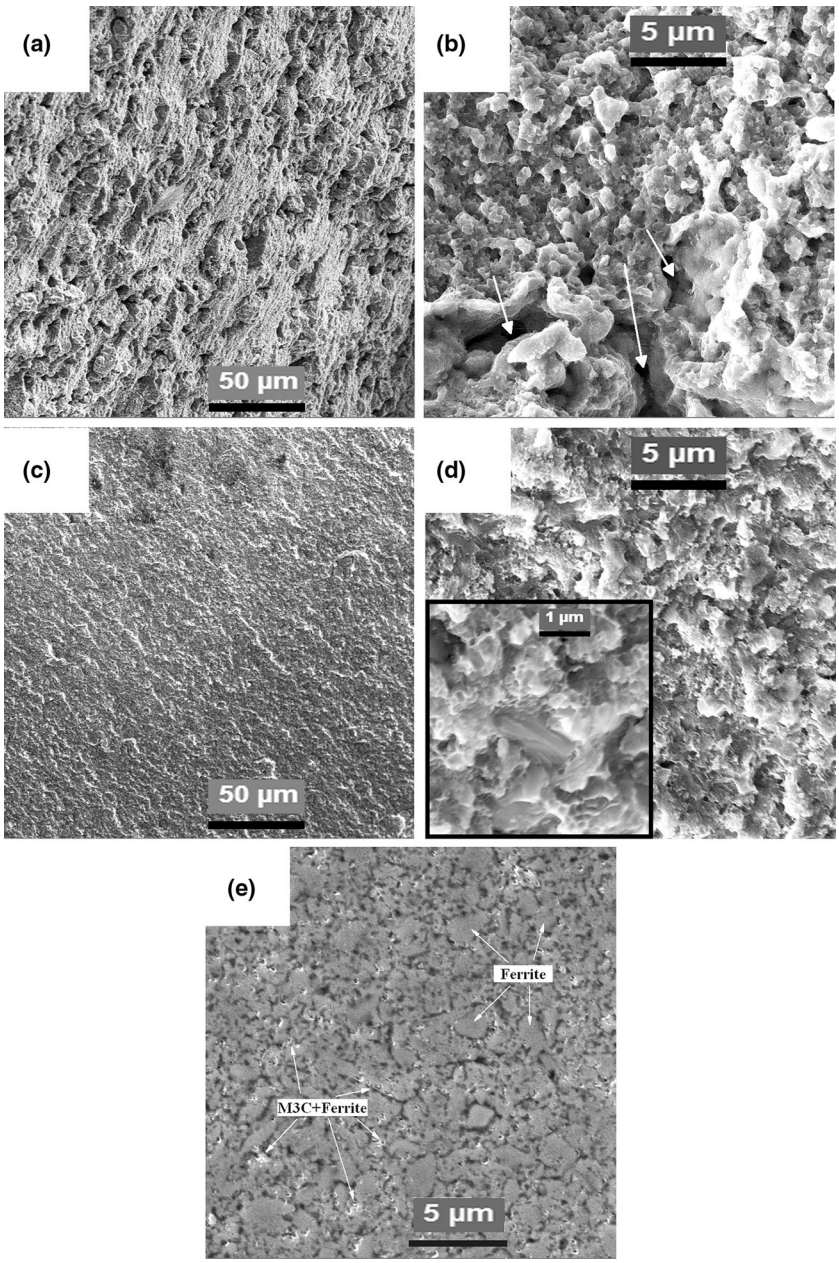

Fig. 6 SEM images: of the fractured surfaces of SPS consolidated **a** C0.25 and **c** C20 steels, high magnification views for **b** C0.25 and **d** C20 and **e** of the mirror polished and etched surface of SPS-consolidated C20

milling [10]. For the P0.25 powder, the increased resistance to compaction of big (Fig. 2a) and hard particles affected its compressibility resulting in a lower density of the SPS-consolidated C0.25 steel; the large spaces between the particles affected as well the Vickers hardness. The reduction in the large interparticle spaces/voids is one of the reasons of the enhancement of both density and hardness in the steels derived from the powders milled with higher amounts of PCA, and more efficient densification was achieved in these steels due to the smaller particle size of the as-milled powders.

The same carbides and oxides precipitated during milling and during SPS consolidation, if they are very fine and uniformly dispersed within the alloy matrix, can increase the Vickers hardness of the steels with the increase in the amounts of PCA. (Table 1 demonstrates an overall increasing trend of hardness.) On the other hand, the precipitation of high quantities of Cr-rich oxides and carbides (in the strained matrix supersaturated with carbon and oxygen) in the steels derived from the powders milled with the highest amounts of PCA caused the decrease in hardness, in particular because of the Cr depletion of the matrix. (In this context, the lattice constant of post-SPS-annealed

steels decreases progressively as the amount of PCA increases (Fig. 5a-inset, Table 1) due to Cr depletion of the matrix caused by the precipitation of high amounts of Cr-containing M_3C and $(Fe,Cr)_2O_3$).) This is evident when comparing the Vickers hardness of C20- and C4-consolidated steels, the hardness of C20 is slightly lower than the hardness of C4 despite the higher amounts of fine carbides and oxides were detected by XRD in the former—17.0(12) mass% of $(Fe,Cr)_2O_3$ with 18.2(25) nm crystallite size and 43.8(15) mass% of M_3C with 18.7(17) nm crystallite size were calculated by Rietveld refinement of XRD of SPS-consolidated C20 steel. The elemental mapping at the microstructural level by SEM with EDS of SPS-consolidated steels (and of as-milled powders) failed to detect any non-homogeneities in the elemental distribution, and no precipitates were detected at any PCA concentration level because their size is under the detection limit. Instead, the SEM micrographs on the etched surfaces (in 2% nitric acid solution) confirm the presence of regions of mixed M_3C—α microstructure in the ferrite matrix of C20 steel as shown in Fig. 6e.

Finally, the rapid cooling of the carbon-rich solid solution from the austenitic field region can result in increased dislocation density associated with phase transformations and interstitial solid solution strengthening [10 and references therein]; this might have contributed to the increase in hardness in the steels derived from the powders with high amounts of PCA (Table 1).

The Vickers hardness of the annealed steels with the relaxed ferrite matrix decreases as compared to SPS-consolidated steels; it maintains the increasingly trend as the amount of PCA increases (Table 1), and it is visibly higher for P20 which contains a high amount of precipitated carbides and oxides. The density has almost not changed after annealing (Table 1).

As already mentioned, the achievability of the local excessive high temperatures, exceeding the nominal (maximum programmed, 1070 °C here) one, at the contact points/particle surface is a characteristic feature for SPS consolidation (e.g., [10, 11 and references therein]). The local excess of heat can reach hundreds of degrees which is much higher than the temperature delay caused by the high heating rate used. In this conditions, the carbothermal reactions described in Eqs. 1–4 can develop at the neck/particle surfaces of Fe14Cr alloy at much lower nominal temperatures (here 1070 °C) during SPS consolidation and can accelerate the densification. These local thermally activated processes are more intense in the products consolidated from the powders milled with a high amount of PCA and thus containing more carbon (carbides) and oxygen (oxides). The carbothermal reduction can facilitate the removal of surface $(Fe,Cr)_2O_3$ oxides allowing the formation of metal–metal sintering contacts [23] between particles improving densification. In addition, a high C concentration at the contact points/particle surface can promote the formation of liquid phases, e.g., the transitions like $\gamma + \text{Carbide} \rightarrow \text{Liquid} + \gamma$ can occur [24]. (More details in this aspect are given in [10] and references therein). The melting and softening of the particle surface promoted by the above-mentioned processes can improve the plastic flow and densification during SPS consolidation.

There is a difference between the XRD of the as-milled powders annealed at 900–1050 °C (Fig. 1b and c) and of the steels with polished surface post-SPS annealed in the same temperature range (Fig. 5a): P20-annealed powder shows $M_{23}C_6$, whereas A20-polished steel contains M_3C; A4-polished steel shows (besides $M_{23}C_6$) traces of reflection of M_7C which were detected in P4 powder heated at lower temperatures, 525 °C. Another difference is that the reflections for carbides (and α-ferrite) are broader for the annealed and polished steels than for the heated powders. On the other hand, XRD measured on the unpolished surfaces of the SPS consolidated and annealed at 900–1000 °C (A4-unpolished and A20-unpolished) steels illustrated in Fig. 5b show narrow reflections (coarse grains) as in the heated powders (Fig. 1b and c). A20 unpolished steel (Fig. 5b) contains the same M_3C carbide as A20 polished steels contain (Fig. 5a), whereas in A4-polished steel (Fig. 5a), the phase composition is similar to that in P4 powder annealed at 900 °C (Fig. 1b). These differences are caused by the different rates of carbothermal reactions in bulks and powders. The C reduction in the bulk steel annealed for 30 min occurred in a layer at the surface which was removed by polishing (Fig. 5a). In bulk steels during furnace annealing under H_2-containing atmosphere, the decarburization is possible [26]:

$$C + 2H_2 \rightarrow CH_4 \quad (7)$$

The reactions (carbothermal, decarburizing) that imply C loss occur with higher rate in powders because of the higher surface-to-volume ratio. The heat treatment in the reducing medium at 900–1050 °C of steel containing M_3C and α-ferrite, the austenite nucleates at M_3C–ferrite interface [26, 27], carbide being dissolved because a higher carbon solubility limit of austenite than ferrite. The released carbon diffuses through the steel matrix to the sample/particle surface where it reacts with the reductant agents/medium with CO or CH_4 degassing. Carbon depletion of the steel matrix near surface leads to the formation of a surface layer of ferrite with coarse grains which thickness increases with the annealing time [28]. Within this layer, M_3C coarsens and its amount decreases gradually to the surface of the sample. The rate of dissolution of M_3C, C depletion and transformation to $M_{23}C_6$ is higher in powder than in bulk steel due to higher surface-to-volume ratio. As a result, the powder P20 annealed at 900-1050 °C

consists of α-ferrite and coarse (narrow reflections in XRD) $M_{23}C_6$ (Fig. 1c), whereas the XRD of bulk steels still shows (coarse) M_3C.

The milling with PCA hinders the contamination with nitrogen

As already discussed, the contamination with nitrogen from milling media and/or air during milling decreases as the amount of PCA increases (Table 2, Fig. 3d). Two factors might contribute to this. (i) Milling with PCA creates a high pressure in the vials in particular because the high temperature evolved in the containers. The created high pressure does not allow the outside atmosphere to leak into the vial during milling even when the integrity of the vial seal is imperfect. The higher the amount of PCA is, the longer time the high pressure is maintained in the vials. This can explain the low contamination level with nitrogen, 0.0323 mass%, of P4 powder (Table 2). (Much smaller amount of nitrogen, 0.0113 mass%, was found in P30 powder milled for short time with 30 mass% PCA.) After the all PCA was disintegrated and dissolved into the powder and/or adsorbed on the powder particle surface, the transition to the "dry milling" occurs; the leak formation and the leakage of air through the seals into the container begin during milling as in the case of dry milling in an Ar atmosphere described in [4]. In the case of low amounts of PCA, the transition to "dry milling" occurred at an earlier stage of milling; this can explain the higher contamination level with nitrogen of P0.25 powder, 0.324 mass%. (ii) It is known that the addition of Cr alloying element enhances the nitrogen uptake in stainless steel. At the same time, a high carbon content hinders the nitrogen incorporation into the steel [28, 29 and references therein]—this was the prevailing factor for low nitrogen content in the powders milled with a high amount of PCA, e.g., very low nitrogen content was measured in the P4 powder. The high Cr (here 14 mass%) and low carbon content can allow the nitrogen to be absorbed [29]. This can explain the high level of contamination of the powders milled with low amounts of (or without) PCA, e.g., a high level of nitrogen was detected in C0.25 (and C0) products (Table 2, Fig. 3d). Therefore, the milling with PCA can serve as an alternative when the contamination with nitrogen is not desired.

Conclusions

Fe–14Cr–3 W–0.4Ti–0.25Y_2O_3 powders were milled with different amounts of ethanol (0.25 mass%, 2.5 mass%, 4 mass% and 20 mass%) in the aim to understand the influence of PCA (carbon and oxygen) on the microstructure, thermal properties, density and Vickers hardness of the as-milled powders and SPS-consolidated steels.

- As the amount of PCA increases the ferritic matrix supersaturates with carbon (and oxygen) with the tendency to precipitate carbides and oxides. The powder milled with the highest amount of PCA, 20 mass%, contains M_3C and oxides $(Fe,Cr)_2O_3$.
- Irrespective of the amount of PCA, the presence of carbon and oxygen in all the products was inferred from the thermal analysis (TG, DTA and MS curves). The increase in the amount of TG mass loss (and the broadening of the temperature range of mass loss) with the increase in the amount of PCA was associated with the increase in CO and CO_2 release. The CO and CO_2 degassing is the result of the carbothermal reaction (e.g., reduction in oxides) with carbides and carbon as reductant agents. (M_3C, $M_{23}C_6$ and $(Fe,Cr)_2O_3$ were detected by XRD in the P2.5, P4 and P20 post-SPS-annealed steels, whereas C and O contaminants were detected in C0.25 and C4 by LECO analysis.)
- The thermally activated phenomena observed in the thermal analysis can develop (locally at the necks/particle surfaces where very high temperatures can exceed the nominal one) during SPS consolidation—this can enhance the densification process and thus the density and Vickers hardness of the final steel.
- Other factors that influence the density and Vickers hardness are: (i) the particle size in the as-milled powders which decrease with the increase in the amount of PCA; (ii) the particle hardness of the as-milled powders which increase with the increase in the amount of PCA due to the presence of interstitial carbon and oxygen and/or fine carbides and oxides precipitates; (iii) Cr depletion of the matrix (supersaturated with carbon and oxygen) caused by the carbides and oxides precipitation and coarsening.
- The decrease in the intensity of the exothermic feature at about 600 °C (associated with nitrides precipitation in the powders milled with the lowest amounts of PCA, e.g., 0.25 mass%) as the amount of PCA increases was ascribed to the decrease in the quantity of the nitrogen uptaken from milling media and/or air which is supported by LECO analysis. This implies that milling with PCA hinders the contamination from air; the explanation for this phenomenon was given. Milling with PCA can serve as an approach for minimizing the contamination from air.
- The results obtained on the products derived from the powders milled with the lowest (known) amounts of PCA can help the understanding of the influence of the contamination with traces of carbon from the container

walls and balls or air during long time—high-energy dry milling (0 mass% PCA) on the properties of the as-milled powders and consolidated steels.
- The results of thermal analysis can help to choose the optimum temperature for degassing, consolidation, annealing and/or for reducing oxides, carbides and nitrides if they are not desired in the steels.

Acknowledgements This work was supported by the CCDI-UEFISCDI PN-III-P1-1.2-PCCDI-2017-0871: Project 47PCCDI/2018 and Core Program PN19-03 (contract no. 21 N/08.02.2019) of Romanian Ministry of Research and Innovation and was partially supported by the European Community in the framework of the European Fusion Development Agreement (EFDA) under project WP13-MAT-01-ODSFS-01. The views and opinions expressed in this paper do not necessarily reflect those of the European Commission. The authors gratefully acknowledge N. Ordas (from Ceit-IK4 and TECNUN, University of Navarra, Spain) for her technical and experimental support.

References

1. Baluc N, Boutard JL, Dudarev SL, Rieth M, Brito Correia J, Fournier B, Henry J, Legendre F, Leguey T, Lewandowska M, Lindau R, Marquis E, Muńoz A, Radiguet B, Oksiuta Z. Review on the EFDA work programme on nano-structured ODS RAF steels. J Nucl Mater. 2011;417:149–53.
2. Shaigan N, Qu W, Ivey DG, Chen W. A review of recent progress in coatings, surface modifications and alloy developments for solid oxide fuel cell ferritic stainless steel interconnects. J Power Sources. 2010;195:1529–42.
3. Herting G, Odnevall Wallinder I, Leygraf C. Corrosion-induced release of chromium and iron from ferritic stainless steel grade AISI 430 in simulated food contact. J Food Eng. 2008;87:291–300.
4. Mihalache V. Thermal analysis of ball-milled Fe–14Cr–3 W–0.4Ti–0.25Y2O3 ferritic steel powder. evidence for contamination from the air. J Therm Anal Calorim. 2016;124:1179.
5. Mihalache V, Mercioniu I, Aldica G, Pasuk I. Thermal analysis, microstructure and impurity phases evolution in Fe14Cr ferritic steel powders ball-milled in air and under an argon atmosphere. J Therm Anal Calorim. 2018;134:463.
6. Suryanarayana C. Mechanical alloying and milling. New York: Marcel Dekker; 2004.
7. Nouri A, Wen C. Critical reviews in solid state and materials. Sciences. 2014;39:81–108.
8. Lü L, Lai MO. Mechanical alloying. Massachusetts: Kluwer Academic Publishers; 1998.
9. Mihalache V, Secu M, Grivel JC. Defect states and room temperature ferromagnetism in cerium oxide nanopowders prepared by decomposition of Ce-propionate. Mater Chem Phys. 2018;209:121–33.
10. Mihalache V, Walter M, Mercioniu I, Ordas N. The quality of $Fe_{14}Cr$ ODS powder alloys during milling and upon heating and its impact on the mechanical properties of consolidated steels. Metall Mater Trans A. 2019;50:3282.
11. Mihalache V, Mercioniu I, Velea A, Palade P. Effect of the process control agent in the ball-milled powders and SPS-consolidation temperature on the grain refinement, density and Vickers hardness of Fe14Cr ODS ferritic alloys. Powder Technol. 2019;347:103–13.
12. Lemoine C, Fnidiki A, Lemarchand D, Teillet J. Grain core study of Fe1–xCrx nanograins obtained by mechanical alloying. J Phys Condens Matter. 1999;11:8341.
13. Fnidiki A, Lemoine C, Teillet J. Structural and magnetic properties of grain boundaries in Fe60Cr40 alloy synthesized by mechanical alloying. J Phys Condens Matter. 2002;14:7221.
14. Azzaza S, Alleg S, Sunol JJ. Microstructure characterization and thermal stability of the ball milled iron powders. J Therm Anal Calorim. 2015;119(2):1037–46.
15. Alleg S, Souilah S, Suñol JJ. Thermal stability of the nanostructured powder mixtures prepared by mechanical alloying. In: Elkordy AA, editor. Applications of calorimetry in a wide context—differential scanning calorimetry, isothermal titration calorimetry and microcalorimetry. Vienna: InTech Publisher; 2013. p. 21–48.
16. Hebda M, Gadek S, Skałon M, Kazior J. Effect of mechanical alloying and annealing on the sintering behaviour of AstaloyCrL powders with SiC and carbon addition. J Therm Anal Calorim. 2013;113:395–403.
17. Calderon RO, Gierl-Mayer C, Danninger H. Application of thermal analysis techniques to study the oxidation/reduction phenomena during sintering of steels containing oxygen sensitive alloying elements. J Therm Anal Calorim. 2017;127:91–105.
18. Kirakosyan H, MinasyanT Niazyan O, Aydinyan S, Kharatyan S. DTA/TG study of CuO and MoO_3 co-reduction by combined Mg/C reducers. J Therm Anal Calorim. 2016;123:35.
19. Hryha E, Nyborg L. Thermogravimetry study of the effectiveness of different reducing agents during sintering of Cr-prealloyed PM steels. J Therm Anal Calorim. 2014;118:825–34.
20. Wang Y, Wang L, Yu J, Chou KC. Kinetics of carbothermic reduction of synthetic chromite. J Min Metall Sect B Metall. 2014;50:15–21.
21. Mori T, Yang J, Kuwabara M. Mechanism of carbothermic reduction of chromium oxide. ISIJ Int. 2007;47:1387.
22. Zhang Yan-ling, Liu Yang, Wei Wen-jie. Carbothermal reduction process of the Fe–Cr–O system. Int J Miner Metall Mater. 2013;20:931.
23. Danninger H, Gierl C, Kremel S, Leitner G, Jaenicke-Roessler K, Yu Y. Degassing and deoxidation processes during sintering of unalloyed and alloyed PM steels. Powder Metall Prog. 2002;2(3):125–40.
24. Zadra M, Molinari A. High carbon nickel-free austenitic steel. Powder Metall Prog. 2005;5:173–84.
25. Hebda M, Debecka H, Kazior J. Dilatometric study of low-alloy steels with silicon carbide addition. J Therm Anal Calorim. 2016;125:1319–26.
26. Alvarenga HD, Van De Putte T, Van Steenberge N, Sietsma J, Terryn H. Influence of carbide morphology and microstructure on the kinetics of superficial decarburization of C–Mn steels. Metal Mater Trans A. 2015;46A:123–33.
27. Inoue A, Masumoto T. Carbide reactions (M3C → M7C3 → M23C6 → MC6) during tempering of rapidly solidified high carbon Cr–W and Cr–Mo steels. Metal Mater Trans A. 1980;11A:739–47.
28. Calliari I, Dabalà M, Ramous E, Zanesco M, Gianotti E. Microstructure of a nitrided steel previously decarburized. J Mater Eng Perform. 2006;15(6):693–8.
29. Sung JH, Kong JH, Yoo DK, On HY, Lee DJ, Lee HW. Phase changes of the AISI 430 ferritic stainless steels after high-temperature gas nitriding and tempering heat treatment. Mater Sci Eng A. 2008;489:38–43.